

Article

Safety Analysis of Synergetic Operation of Backfilling the Open Pit Using Tailings and Excavating the Ore Deposit Underground

Qinli Zhang, Bingyi Zhang, Qiusong Chen *, Daolin Wang and Xiang Gao

School of Resources and Safety Engineering, Central South University, Changsha 410083, China; zhangqinlicn@126.com (Q.Z.); zhangbingyicsu@163.com (B.Z.); daolinw@csu.edu.cn (D.W.); xiang_gao4@Shimaogroup.com (X.G.)

* Correspondence: qiusong.chen@csu.edu.cn; Tel.: +86-151-1627-9873

Abstract: The transition from open pit mining to underground mining is essential for mineral resources to achieve deep excavation. Recently, cemented paste backfill (CPB) has been proposed as a novel technology to achieve open pit backfill (OPB). The proposed method not only eliminates the danger of the open-pit slope but also reduces the disposal of waste tailings. In order to ensure safe mining during the synergetic operation of OPB and underground mining, it is of great significance to improve this technology. In the present study, an open-pit metal mine in Anhui Province was taken as the research object. Then, the safety of underground stope roofs, underground backfill pillars, and open-pit slopes was evaluated during OPB. To this end, numerical simulations were performed and experiments were conducted on a similar physical model. Accordingly, the backfill mechanical parameters were optimized. The obtained results show that backfill height exerts the most significant effect on the safety of roofs and underground backfill pillars, accompanied by small displacements along the vertical direction during the backfill process. Moreover, concentration was observed at the foot of the slope, while the overall structure remained stable with no considerable displacement. The overall safety factors met the safety requirements. Based on the obtained results, the optimal foundation strength, foundation height, backfill strength and backfill height were 4 MPa, 10 m, 1.5 MPa, and 120 m, respectively. Moreover, it was concluded that displacements in the abovementioned three regions tend to be stable when the backfill height exceeds 150 m without damage. The present article provides a certain theoretical and application guideline for OPB practices in similar metal mines and suggests possibilities for cleaner production.

Keywords: cemented paste backfill; backfill strength; transition from open pit to underground mining; tailings disposal; numerical simulation



check for updates

Citation: Zhang, Q.; Zhang, B.; Chen, Q.; Wang, D.; Gao, X. Safety Analysis of Synergetic Operation of Backfilling the Open Pit Using Tailings and Excavating the Ore Deposit Underground. *Minerals* **2021**, *11*, 818. <https://doi.org/10.3390/min11080818>

Academic Editor: Abbas Taheri

Received: 7 July 2021

Accepted: 26 July 2021

Published: 28 July 2021

Publisher's Note: MDPI stays neutral with regard to jurisdictional claims in published maps and institutional affiliations.



Copyright: © 2021 by the authors. Licensee MDPI, Basel, Switzerland. This article is an open access article distributed under the terms and conditions of the Creative Commons Attribution (CC BY) license (<https://creativecommons.org/licenses/by/4.0/>).

1. Introduction

Considering reasonable economic parameters (such as stripping ratio) in the mining industry, it is crucial to transition from the open pit to the underground mining after reaching the 'great depth' in open-pit metal mines [1]. Such conversion can make full use of existing infrastructures and equipment to facilitate the excavation of ore deposits, which is of great significance for the sustainable development of metal mines. Further investigations reveal that the open pit caused by the open-pit mining not only threatens the local environment, but the created puddle affects the safety of the underground mining. On the other hand, it increases occurrence probability of collapses and landslides (Figure 1a), thereby becoming a major source of safety hazards during the normal operation of metal mines [2].

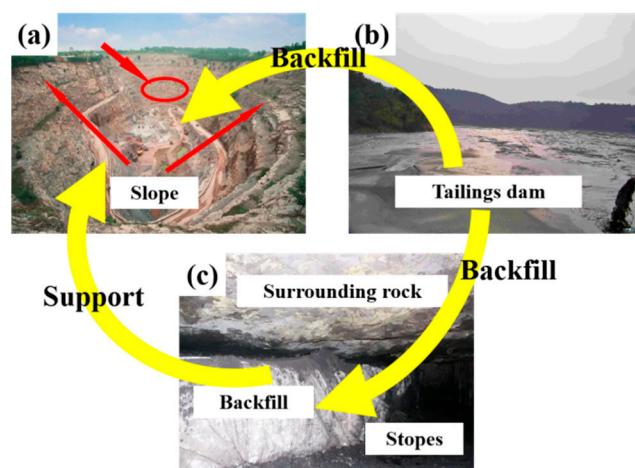


Figure 1. Relationship between slopes (a), tailings dam (b), and stopes (c) in surface and underground mining.

In the past few decades, increasingly large quantities of mine tailings have been produced as a result of excavating mineral resources [3,4]. Furthermore, more than 120,000 tailing dams have been established worldwide to deposit about 25 billion tons of untreated mine tailings (Figure 1b), resulting in the contamination of large amounts of Earth's surface and water, respectively [5]. A tailing dam, as a place to store mine tailings, has many drawbacks, such that establishing new tailing dams is not allowed in many countries. On the other hand, the comprehensive utilization rate of the mine tailing in China is less than 30% [6,7]. Consequently, it is necessary to increase the disposal efficiency of mine tailings. Recently, cemented paste backfill (CPB) has been proposed as an innovative technology to fill mined-out voids (also known as stopes) and effectively reduce environmental damages originating from tailing piles on the ground surface (Figure 1c). The scheme, which consists of a binder (e.g., cement), aggregates (e.g., mine tailings), and mixing water [8] can be effectively applied to eliminate hazards in underground stopes and improve the safety of underground mining operations, especially the recovery of ore bodies. Figure 1 illustrates the relationship between slopes, tailings dam, and stopes.

CPB is the most eco-friendly method to resolve tailings problems [9]. Therefore, it should be adopted to fill the open pit. It cannot only solve challenges originating from the disposal of mine tailings, but can also provide conditions for subsequent ecological restorations in open pits. Reviewing the literature on the subject indicates that the CPB method has been successfully conducted in some metal mines under different conditions. For instance, Lu et al. (2018) applied tailings to backfill the open pit of Shirengou Iron Mine (SIM), which realized 100% utilization of waste tailings and achieved clean production for its mining. Additionally, a method was proposed to combine the desulphurization technology and CPB, which can improve the disposal of waste tailings and support for surrounding rocks [10]. Simultaneously, an open pit mine planning stochastic integer program with tailings disposal was established and applied at an iron ore deposit located in Labrador, Canada, which can greatly contribute to ore production and disposal of tailings [6]. Nevertheless, there is no comprehensive specification or standard to implement with respect to OPB, which leads to a lack of evidence on the influence of its practice on slopes, roofs and underground backfill pillars when OPB is processing. In order to resolve this shortcoming, this issue is considered as the research object of the present study.

In this article, an open pit in Anhui was considered as the case study. It has a length of 1250 m, a width of 500 m, a volume of about 43 million cubic meters. Its highest slope has a height of 482 m. In order to accomplish rational disposal and ecological restoration of the open pit, metal mine tailings were used for OPB. Since the metal mine is in the transition stage from open pit to underground mining, safety issues have become the key factor in the implementation of this project. Therefore, this research aims to analyze the safety

of synergetic operation of backfilling the open pit using tailings and excavating the ore deposit underground, including the stability of slopes, roofs, and underground backfills. Noted that the study does not take into account the possibility of a hazardous impact of CPB on groundwater due to toxic components in tailings. The present article is expected to provide a basis for OPB and eco-friendly production of metal mineral resources.

2. Methods and Proposals

2.1. Study Site

The present study is focused on an open-pit metal mine from the open pit to the underground mining in Anhui province, China. The metal mine is located in the middle section of the copper-iron metallogenic belt in the middle and lower reaches of the Yangtze River. The geotectonic structure belongs to the Ma'anshan-Guichi fault fold belt of the Lower Yangtze depression fold belt. The main strata exposed in the mining area are Silurian, Upper Devonian, Carboniferous, Permian, and Quaternary. The strata in the eastern part of the mining area strikes northeast and tends to northwest, with an inclination of 45° or more in the upper part and about 20° in the lower part.

In the studied mine, a two-step mining method was utilized. The first step consists of a 15 m wide room, followed by a 10 m pillar in the second step, which perceives excavated pillars from bottom to top in a layered form. Then, CPB is filled to create a platform, allowing upward mining operation. Figure 2 presents the schematic diagram of the studied open pit. When pillars are mined and filled by CPB, the same process is performed to excavate the CPB-filled room. It should be noted that the ore bodies to be excavated are below the -156 m level. In particular, the ore bodies in the middle section of -380 m are mined first, and then the middle section of -320 m, -270 m, and -230 m is mined, respectively, leaving a boundary pillar of 24 m high between the -180 m and -156 m levels.

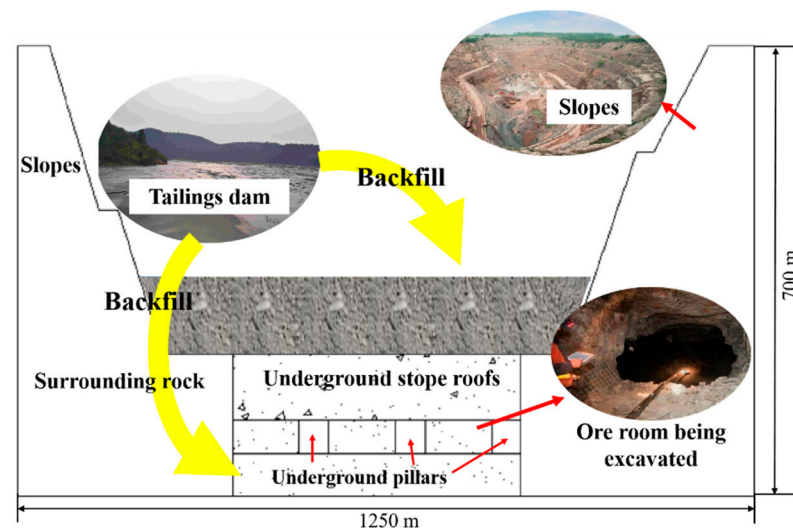


Figure 2. Open pit and underground stopes.

Due to the open pit and high-steep slope caused by the open-pit mining shown in Figure 2, a great risk threatens the entire excavation process of lower ore bodies. This process may also affect the stability of the slope [11]. Accordingly, it is necessary to consider the stability of underground stopes (including roofs and underground backfill pillars) and the slope to prevent geological disasters. In engineering practices, tailings, cement and mixing water in a certain proportion are transported to the filling slurry preparation station through pipelines to prepare homogeneous slurry by utilizing mixing equipment, which will be transported to underground stopes and the open-pit through the pipeline system.

2.2. Numerical Simulation Tests

Among different numerical methods, explicit finite volume analysis has the advantages of its simple process, which can reflect dynamic parameters such as stress and strain [12]. In the present study, post-processing and explicit finite volume analysis of Flac3D 6.0 software are employed to simulate and analyze the stability of the roofs, underground filling column, and slopes during the underground mining at different backfilling conditions. Moreover, the elastoplastic material model and the Mohr-Coulomb strength criterion were used to evaluate the stability [13,14].

The principal stress, which is the main parameter in rock mechanics, can be expressed in the form below [15,16]:

$$\sigma_3 = \sigma_1 \tan^2(45^\circ - \varphi/2) - 2c \cdot \tan(45^\circ - \varphi/2) \quad (1)$$

$$f = \frac{\sigma_3}{\sigma_3'} \quad (2)$$

where σ_1 is the maximum principal stress (compressive stress is negative and tensile stress is positive), MPa; σ_3 is the theoretical minimum principal stress, MPa; σ_3' is the calculated minimum principal stress, MPa; φ denotes the internal friction angle of the material, °; and f is a safety factor. When $f < 1$, damage will occur.

Boundary conditions conducted in this model are as follows. In the numerical simulation calculation, the horizontal displacement of the left and right boundaries of the model was fixed, the displacement at the bottom of the model was fixed, and the top of the model was set as a free surface. In terms of boundary stress, trapezoidal stress was applied to the left and right of the model. The effects of boundary conditions on the results of the numerical simulation can be ignored.

2.2.1. Modeling

A numerical model of OPB was established in the Flac3D environment. Figure 3 indicates that dimensions of the model along X-, Y- and Z-axes are 1250 m, 500 m, and 700 m, respectively. It is worth noting that an ideal elastoplastic body was selected as the ore rock mass to simplify the analysis, which ignored slight differences between ore rock mass components to simplify the simulation process. In this regard, the backfills are assumed to be in close contact with the surrounding rock and fully connected to the top after slopes are filled. In other words, the effect of “saw-tooth” reinforcement of the backfill on the slope steps is ignored. Moreover, two test schemes with different total backfill heights were subjected to the test to reflect the safety effect on each region during the OPB operation.

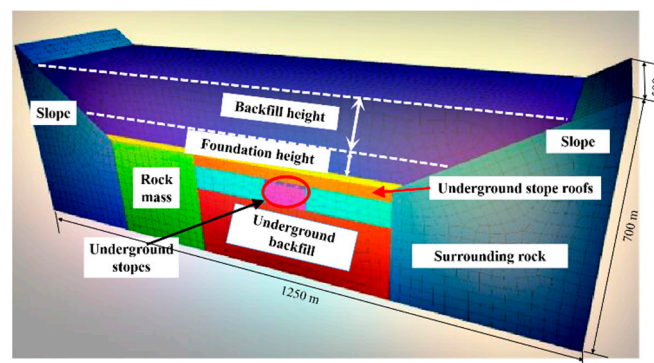


Figure 3. Numerical model.

2.2.2. Parameters

Considering the existing geological data of the studied mine and experiments of CPB, the mechanical parameters of the ore rock and underground backfills are summarized

in Table 1. Furthermore, Supplementary Table S1 presents the backfill parameters of the open pit.

Table 1. Mechanical parameters of underground mining rock and underground backfill.

Materials	Elastic Modulus (GPa)	Poisson's Ratio (μ)	Density (t/m^3)	Compressive Strength (MPa)	Tensile Strength (MPa)	Cohesion (MPa)	Internal Friction Angle ($^\circ$)
Granite	33.81	0.26	2.73	50.38	4.16	6.23	41.20
Sandstone	8.33	0.26	2.71	17.60	7.05	4.54	34.50
Pyrite	10.20	0.18	3.83	13.20	1.57	3.68	40.70
CPB*	0.185	0.28	1.92	2.20	0.28	0.31	41.91

Note: Granite, sandstone, pyrite and CPB* represent the slope rock, underground rock, ore body, and underground backfill, respectively.

2.2.3. Simulation Schemes

In the present article, a two-step mining process was applied to analyze the stability of the abovementioned three regions with the highest risks during underground mining [17]. The top pressure corresponding to the applied parameters was calculated. Based on the engineering experience, four factors, including the foundation height, foundation strength (28 d), backfill height, and backfill strength (28 d) were selected in calculations through orthogonal experiments. This foundation represents a high-strength backfill filled at the bottom of the open pit. 'Backfill' of 'backfill strength and height' in the factors selected is denoted as backfills above the foundation, which has lower strength compared with the foundation [18]. Based on the construction guideline for reinforced cemented tailings backfill, each parameter was divided into five levels (as shown in Table 2).

Table 2. Backfill parameter level.

Level	Foundation Strength (MPa)	Foundation Height (m)	Backfill Strength (MPa)	Backfill Height (m)
1	2.0	4	0.5	100
2	2.5	6	1.0	120
3	3.0	8	1.5	140
4	3.5	10	2.0	160
5	4.0	12	2.5	180

2.3. Physical Model

In order to investigate the safety of the roofs, underground backfill pillars and the slopes during the backfilling process of the open pit, a physical model was prepared according to the procedure proposed by previous research [19,20]. Moreover, an orthogonal test method was adopted to design a test scheme for similar materials, and investigate stress and displacement at the roof, underground backfill, and the slope under different backfill parameters [21].

2.3.1. Similar Materials

The selection of similar materials plays a crucial role in the physical model. Based on the similarity principles [22,23] and characteristics of materials, barite powder and quartz sand were chosen as aggregates. Cement (ordinary Portland cement 425#), gypsum, and sawdust were used as binders and an additive to conduct similar material tests (Figure 4). The five materials mentioned above were all obtained from a material building factory in Changsha. Meanwhile, C_ρ , C_g , C_θ , C_E , and C_σ were defined the as similarity ratio of the density, acceleration of the gravity, internal friction angle, elastic modulus, and stress, respectively. These values are summarized in Table 3.

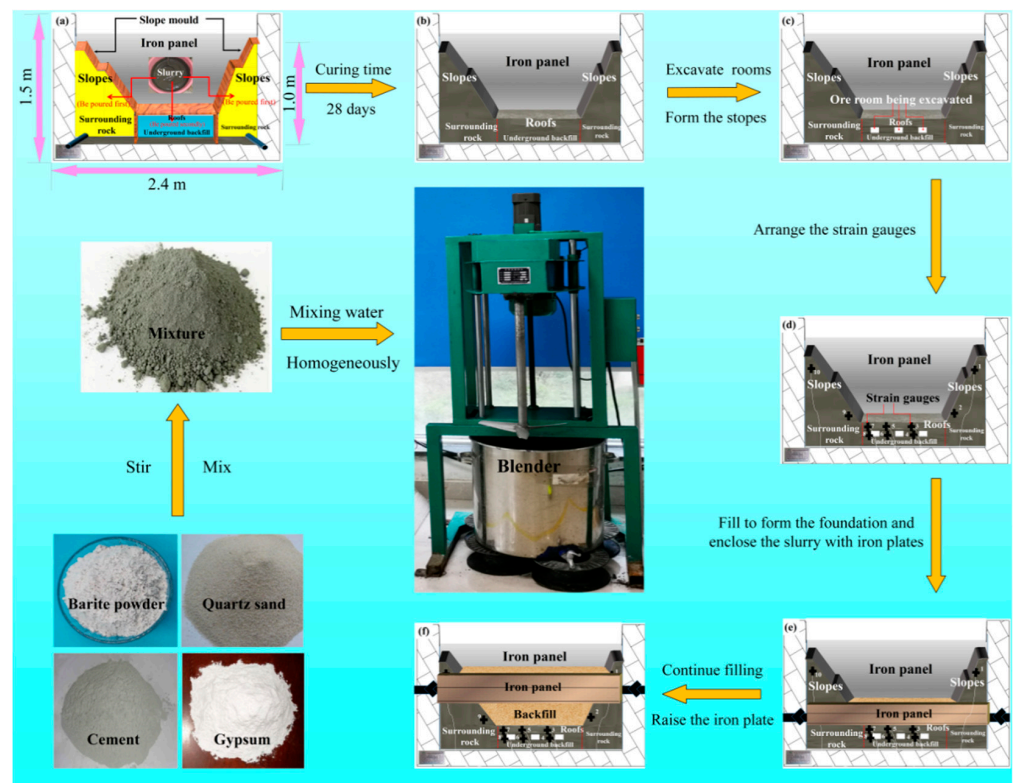


Figure 4. Schematic diagram of the modeling process (a–f).

Table 3. Similarity ratios.

Similarity Ratio	Value
C_ρ	1
C_g	1
C_θ	1
C_E	190
C_σ	190

2.3.2. Parameters

The ideal mechanical parameters of each part of the model can be determined by the similarity principle. Supplementary Table S1 presents the relevant mechanical parameters. The uniform test was performed to select proper similar materials [24]. In this regard, four factors, including the masses of the barite powder, sand, gypsum and cement are considered. Meanwhile, 12 levels and corresponding results of uniform tests are considered and shown in Supplementary Tables S2 and S3, respectively. The main objective of these levels is to control similarity ratios, thereby determining the optimal plan accurately and minimizing the calculation error. The calculations were conducted with different mechanical parameters, including density, elastic modulus, compressive strength, internal friction angle and adhesion force [19]. Then, the obtained results were compared with ideal mechanical parameters. Accordingly, appropriate parameters and the corresponding similarity ratios of the model components were selected as shown in Table 4.

Table 4. Comparison of mechanical parameters of surrounding rock, ore body, underground backfill prototype materials, and similar materials.

Region	Parameters	Prototype Material	Similar Material	Actual Similarity Ratio	Theoretical Similarity Ratio
Surrounding rock	Cohesion (MPa)	6.23	0.038	163.95	190
	Internal friction angle (°)	41.2	41.2	1.00	1
	Compressive strength (MPa)	50.38	0.28	179.93	190
	Density (kg/m ³)	2730	2190	1.25	1
Ore body	Cohesion (MPa)	3.68	0.02	184.00	190
	Internal friction angle (°)	40.7	37.6	1.08	1
	Compressive strength (MPa)	13.2	0.1	132.00	190
	Density (kg/m ³)	3830	2740	1.40	1
Underground backfill	Cohesion (MPa)	0.31	-	-	190
	Internal friction angle (°)	41.91	37.7	1.11	1
	Compressive strength (MPa)	2.20	-	-	190
	Density (kg/m ³)	1920	2180	0.88	1

It should be noted that the effect caused by a difference between theoretical and actual similarity ratios on tests results can be regarded as negligible.

2.3.3. Modeling Process Modeling the Open Pit

In this section, the rock mass plane similarity model test system (ZYDL-YS120) was used to establish the physical model shown in Figure 4a [20]. In the present study, the model height and length of the slope were set to 1.0 and 2.0 m, respectively. It can be observed that the densities of similar materials of surrounding rock (2190 kg/m³) and underground backfill (2180 kg/m³) are similar in value. Based on the parameters of the selected proportions (Supplementary Table S3) and results obtained from numerical simulations, mixtures of schemes 8, 12, and 8 were chosen as materials of the surrounding rock, ore body and underground backfill, respectively. As can be seen in Figure 4, materials were mixed and stirred for 15–30 s by the blender to prepare a homogeneous slurry with a water-to-binder ratio of 0.5 in accordance with Chinese national standard GB/T 12957-2005 and the reference test [25]. Several wooden boards were combined as molds to construct the slope, as shown in Figure 4a. The slurry was first poured into the slopes regions on both sides. After the slurry became hardened, the region in the middle was filled. After 28 days of curing in an environment with a temperature of 25 ± 2 °C and a humidity of 90%, molds were removed (Figure 4b) and the ore rooms in the underground stope were excavated using a concrete cutter with diamond saw blades (500-type) to provide in-situ conditions for underground mining (Figure 4c). Three regions, including the roofs, underground backfill pillars, and slopes, were arranged as main monitoring points to determine the strain development during the OPB operation. Then two strain gauges were installed horizontally and vertically at 10 points to reflect the horizontal and vertical strain at these measuring points (Figure 4d) [26].

OPB

Based on the obtained results from the numerical simulations, which will be discussed in Section 3, the mixtures of schemes 11 and 4 (Supplementary Table S3) were selected for foundation and backfill materials, respectively. It is pertinent to note that the slurry, which

will be filled into the open pit, should also be mixed well and stirred homogeneously. Then it is poured into the open pit with a height of 5 cm, which corresponds to the foundation height of 10 m. Two iron plates of suitable sizes were fixed on the model at the same height as the OPB operation by appropriate clips to prevent the slurry from flowing out (Figure 4e). When the slurry gradually hardened, the initial strain value was adjusted consistent with the strain value at the end of the pouring to maintain the continuity of the strain curve. In order to observe strain trends of the OPB process in different stages clearly and facilitate the management and implementation of OPB, backfill heights were divided into 100, 40, and 40 m levels to reach the maximum OPB height of 190 m. In this way, the corresponding heights of 53, 21, and 21 cm can be calculated. This issue is presented in Figure 5, where stages 0 to 4 reflect the total OPB heights of 10, 110, 150, and 190 m, respectively.

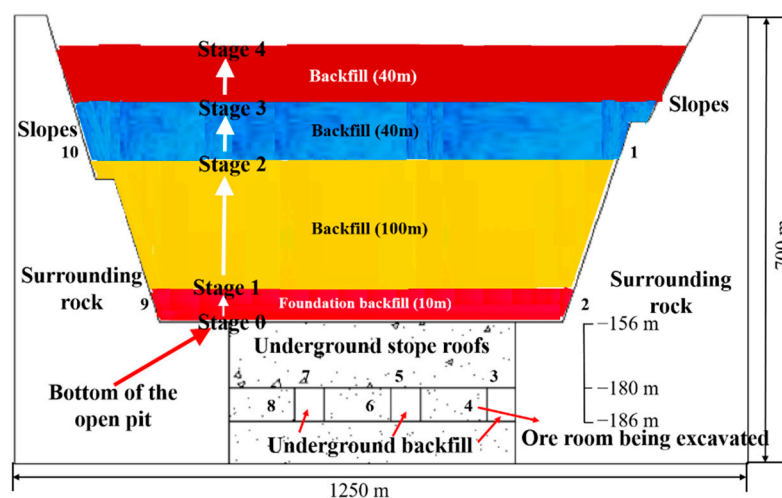


Figure 5. Schematic diagram of backfilling level.

In all experiments, a resistance strain soil pressure cell (BYD-1 type, Sanda Test Instrument, China) was applied to gather the strain data during OPB with a sampling frequency of 2 Hz (In the Section 3, the displacement is used to characterize the change in strain). Sampling was conducted until the maximum OPB height was finished. These steps were repeated constantly to achieve OPB sequentially to 58, 79 and 100 cm, and the iron plates was placed in the same way and raised constantly to the corresponding heights, which were consistent with the height of the OPB (Figure 4f). Finally, the model was cured under the same conditions for 28 days, when the mixtures hardened clearly.

3. Results and Discussion

3.1. The Influence of OPB on the Stope Roofs

Supplementary Table S4 presents the results of the numerical simulation. According to the safety factors of the roofs obtained from Equations (1) and (2), Table 5 shows the analysis of the variance (ANOVA) of the orthogonal test results [27]. In these analyses, F_1 can be coded as the Fisher value, which is called the F-value of the roofs obtained by the numerical simulation. The meanings of sum of square, degree of freedom, and mean square can be obtained in the related literature [28].

It should be indicated that the ANOVA selects 0.05 as the significance level (e.g., the reliability is more than 95%) to meet the analysis requirements. Searching in the Fisher distribution (referred to as F-distribution from statistical distributions according to GB 4086.4—83) shows that an $F_{0.05}(4, 8)$ value of 3.84 can be obtained.

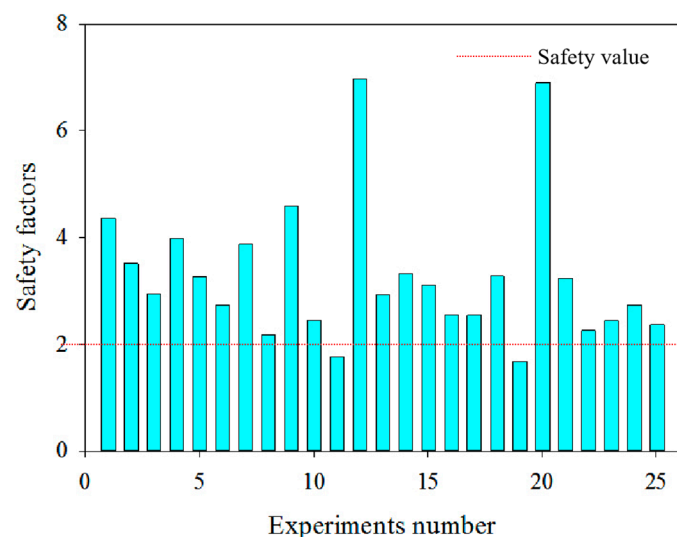
Table 5. The ANOVA of the safety factor of the roofs obtained by the numerical simulation.

Source of Variance	Sum of Square	Degree of Freedom	Mean Square	F ₁
Foundation strength (A) (MPa)	3.5259	4	0.88149	0.94
Foundation height (B) (m)	4.1103	4	1.02759	1.1
Backfill strength (C) (MPa)	3.0371	4	0.75929	0.81
Backfill height (D) (m)	23.7268	4	5.93171	6.35

Significance $D > B > A > C$.

3.1.1. The Stress Change

Based on the results of ANOVA provided in Table 5, it is observed that only the F-value of the backfill height (i.e., 6.35) is greater than 3.84. Therefore, the backfill height from 100 to 180 m significantly affects the safety factor of the roofs, while others have a smaller impact than that of backfill height on roofs. The significance weight ranking of four factors is: $D > B > C > A$ (Table 5), which demonstrates that special attention should be paid to backfill height in the process of engineering practice to prevent negative effects on safety. Simultaneously, the trend of safety factors obtained is shown in Figure 6.

**Figure 6.** Safety factors of the roofs obtained by numerical simulation.

3.1.2. The Displacement Change

Figure 7 shows the overall displacement distributions of the model established in the horizontal and vertical directions. Figure 7a,b show that subsidence is inevitably caused on the roofs with the excavation of underground ore bodies, which is consistent with the results obtained by previous studies [29,30]. Moreover, it is found that the maximum downward displacement, which is 6.18 cm, is obtained at the center of the roofs corresponding to the center of stopes, which gradually decreases towards both sides.

3.1.3. Displacement Change in the Similar Model

Figure 8a,b show that from stage 0 to 2, the vertical displacement at point 5 increases as the height of OPB increases. It is found that the growth rate is initially higher, while it maintains a lower rate from stages 3 to 4. Therefore, the maximum displacement of 23.6 cm is obtained and the displacement value gradually becomes stable. Considering the horizontal displacement, it is found that from stages 0 to 2, the displacement produced by point 5 is consistent with that of the vertical displacement. It is worth noting that the maximum displacement of 14.2 cm is obtained during stages 3 to 4. Furthermore, no

damage such as cracks and collapse, are found during the test. Therefore, the application of the proposed OPB cannot affect the safety of the roofs.

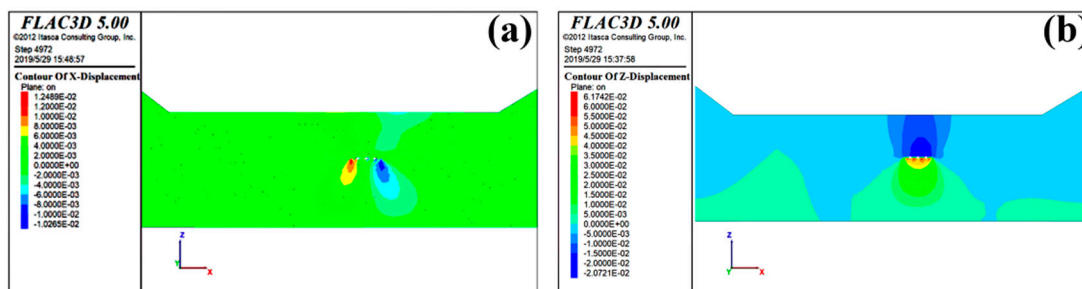


Figure 7. The overall displacements distributions in the horizontal (a) and vertical (b) directions.

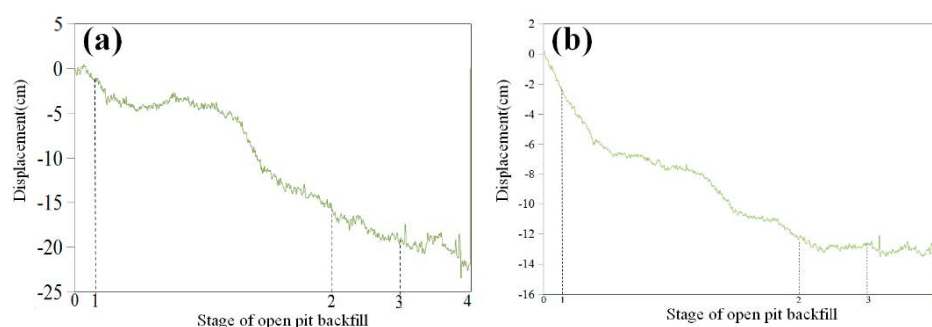


Figure 8. Displacements of measuring point 5 in the vertical (a) and horizontal (b) directions.

In Figure 6 and Supplementary Table S4, it should be noted that the values of safety factors in scheme 11 and 19 are lower than safety value, which is defined as the optimum factor of safety (The safety value is 2) according to safety requirements, demonstrating that these two options should not be allowed in situ application. However, obtained results show that OPB in underground mining does not threaten roofs, although certain stress and displacements are produced during this process [31].

3.2. The Influence of OPB on the Underground Backfill Pillars

3.2.1. The Stress Change

According to the safety factors of underground backfill pillars in Supplementary Table S4 and Figure 9, the results of ANOVA are summarized in Table 6. Where F_2 represents the F-value of the underground backfill pillars obtained by the numerical simulation with the same analysis conditions as roofs.

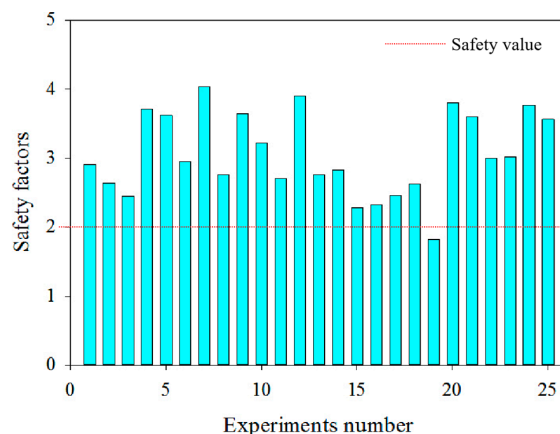


Figure 9. Safety factors of the underground backfill pillars obtained by numerical simulation.

Table 6. The ANOVA of the safety factor of the underground backfill pillars obtained by the numerical simulation.

Source of Variance	Sum of Square	Degree of Freedom	Mean Square	Value of F_1
Foundation strength (A) (MPa)	2.06478	4	0.51620	2.68
Foundation height (B) (m)	1.13730	4	0.28433	1.48
Backfill strength (C) (MPa)	2.17322	4	0.54331	2.82
Backfill height (D) (m)	1.63822	4	0.40956	2.13

Significance $C > A > D > B$.

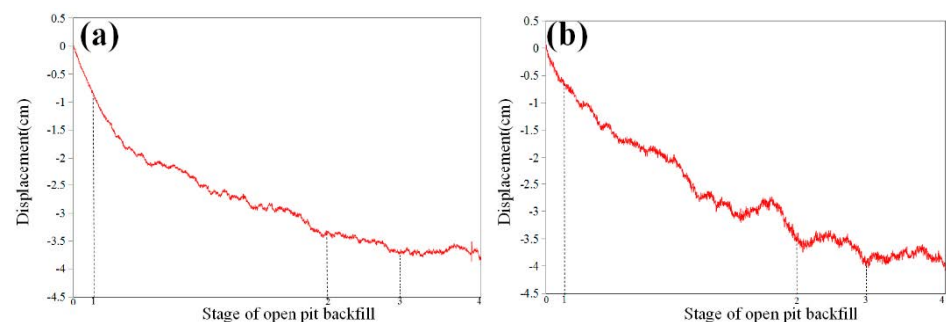
Table 6 presents a fact that the F-values of all factors are less than 3.84. Therefore, the abovementioned factors slightly affect the safety and stability of the underground backfill pillars. This can be explained by the fact that a certain isolation effect is caused by roofs as an isolation layer. Therefore, the disturbance is weakened to underground backfill pillars [32].

3.2.2. The displacement Change

Figure 7 illustrates that larger displacements (6.1742 cm in the vertical direction) of the underground backfill pillars are produced in the vertical direction, which can be explained by the fact that underground backfill pillars have smaller stiffness than that of the surrounding ore bodies [33]. However, the overall structure is stable.

3.2.3. Displacement Change in Similar Model

Figure 10a,b show that as OPB progresses during stage 0 to stage 2, the pressure brought by increasing CPB gradually increases, leading to increased vertical displacement. Moreover, it is found that the displacement slightly fluctuates in the vertical direction when the OPB progresses from stages 2 to 3, and then it gradually rises. During stages 3 to 4, it levels off, with a maximum displacement value of 3.8 cm. It should be indicated that the horizontal displacement is mainly concentrated in stages 0 to 2. However, significant fluctuation can be found, resulting in the increased overall displacement. When entering stage 2, the horizontal displacement increases gradually at a declined rate. When entering stage 3, it remains stable with the maximum displacement value of 3.88 cm.

**Figure 10.** Displacements of measuring point 6 in the vertical (a) and horizontal (b) directions.

Based on the analysis of underground backfill pillars, it is found that the implementation of OPB will not exert a destructive effect on underground backfill pillars under conditions, which are consistent with roofs, despite the larger vertical displacements. However, the perfect integrity of a similar physical model can be observed. As revealed by Figure 9 and Supplementary Table S4, it is worth noting that the value of safety factor in scheme 19 is less than the safety value, which should be paid attention to in engineering operations.

3.3. The Influence of OPB on the Open-Pit Slopes

3.3.1. The Stress Change

Figure 11 presents the maximum and minimum principal stress distributions of the slopes of the open pit in the present study. In order to facilitate modeling, the inclination of the slope in Figure 11 does not seem to be as steep as that in Figures 2 and 5. Since it does not affect the final analysis, this difference can be ignored. It is observed that stress is mainly concentrated at the slope foot. However, the stress (1 MPa) can be found at the top of the slope, which conforms to the general principle of slope deformation [11]. As the height of OPB continuously increases, the stress concentration becomes more apparent and is accompanied by the expansion of the radiation range. Moreover, it is found that compressive stress is distributed in layers in the direction of gravity, which is consistent with the general discipline of compressive stress field distribution described by relevant literature [34]. Despite the concentration of the compressive stress in the slope foot, the overall structure can remain stable and does not cause hazards to the sloping rock, which is consistent with the previous study [35].

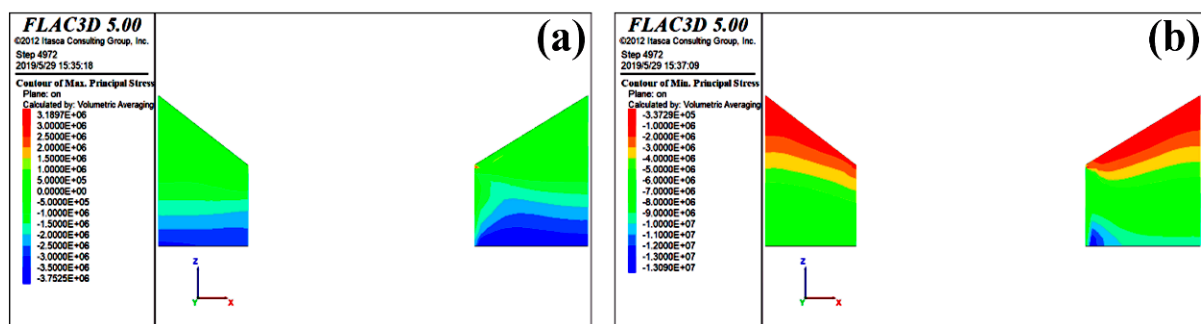


Figure 11. Slope: maximum (a) and minimum (b) principal stress distributions.

3.3.2. The Displacement Change

Figure 7 shows that no obvious displacement is produced on the slopes of both horizontal and vertical directions. This is the result of the reinforcement for slope foot given by overlying CPB, enhancing the anti-sliding force of the slopes. Therefore, the structure is more stable. The mechanism of stability and safety is discussed in the related literature [36].

3.3.3. Displacement Change in the Similar Model

Figure 12a shows that during stages 0 to 2, the vertical displacement gradually increases, and then becomes stable accompanied by sharp increments in displacement, which can reach up to 19 cm. This phenomenon is explained by errors during data measurement. The displacement fluctuates slightly and subsequently levels off. Therefore, when the height of OPB reaches a certain value, it acts as a support for the slopes on both sides which is, in turn, responsible for the gradual disturbance reduction on the slopes. Figure 12b shows that with the continuous filling of the open pit, the horizontal displacement of point 1 is sensitive to the change of the backfill height to a great extent, resulting in a continuous increase in the displacement. Moreover, it is found that the horizontal displacement fluctuates more than the vertical displacement of point 1. This phenomenon accounts for the fact that the slope angles on both sides affect part of the stress provided by the overlying CPB.

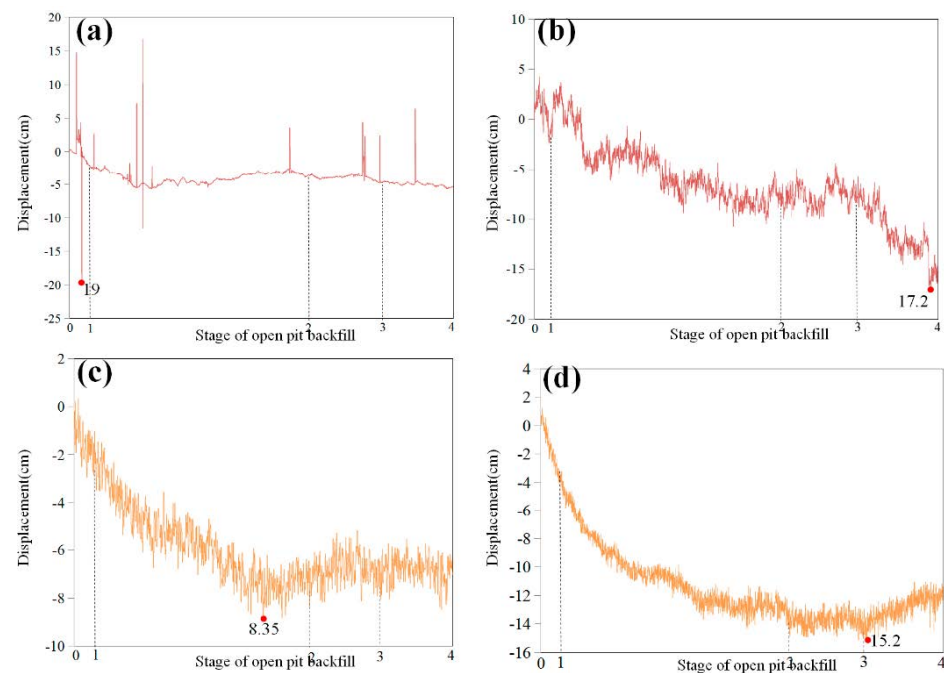


Figure 12. Displacements of measuring point 1 (a) vertical, (b) horizontal, and 2 (c) vertical, (d) horizontal.

Figure 12c shows the vertical displacement of point 2 increases as the height of OPB increases, obtaining a maximum displacement value of 8.35 cm. Then, it decreases slightly after the low point during stages 1 to 2, subsequently fluctuating steadily. In Figure 12d, the horizontal displacement of point 2 demonstrates a similar trend to its vertical displacement as revealed by Figure 12c. However, it is observed that the curve was smoother than that in Figure 12c. Therefore, there is a more stable rate of displacement change. Furthermore, at the beginning of stage 3, the maximum displacement value is obtained, which can reach 15.2 cm.

It is worth noting that the stress and displacements of the slopes can be restricted within a certain range, despite the presence of stress concentration. Therefore, the safety and stability of the slopes are verified.

According to the analysis of numerical simulation on the roofs, underground backfill pillars and slopes, the safety of the abovementioned three regions can be ensured significantly. Considering the use of OPB in many metal mines and relevant costs [37–42], selected parameters of OPB are foundation strength, foundation height, backfill strength and backfill height, which are 4 MPa, 10 m, 1.5 MPa, and 120 m, respectively. Moreover, corresponding safety factors obtained from the roofs and underground backfill pillars are 2.74 and 3.77, respectively, which meet the safety requirements. A similar physical model is investigated to verify whether selected parameters of OPB are reliable based on the numerical simulation. The results confirm that the disturbance effects on the three regions mainly occur before the OPB height is between 110 and 150 m. It should be indicated that no damage, such as cracks or collapse, was found during the test. Therefore, the application of the proposed method in the open pit does not affect the safety of the overall structure.

Comparing numerical simulations with similar physical model tests, it can be concluded that the results of the two are generally similar. It should be noted that similar physical model experiments can verify the accuracy of the numerical simulation results more intuitively.

4. Conclusions

In the present study, a technology named CPB is proposed, which has been used to fill open pits. Numerical simulation is performed to analyze the stress and displacement in the three mentioned areas. Moreover, the safety and stability during the process of

OPB are verified by physical model tests. The following conclusions are drawn from the present study:

- (1) Comprehensive analysis is obtained through ANOVA. Among the factors affecting the roofs and underground backfill pillars, the backfill height plays a significant role in roofs and underground backfill pillars. Moreover, the obtained safety factors meet the requirements. In other words, the safety of the roofs and underground backfill pillars during OPB is guaranteed. It should be indicated that the foundation strength, foundation height, backfill strength, and backfill height are 4 MPa, 10 m, 1.5 MPa, and 120 m, respectively.
- (2) The displacement gradually stabilizes when the backfill height is greater than 150 m. Moreover, no cracks or other damage appears, which verifies the reliability and accuracy of obtained numerical simulation results attained. In other words, the safety of the main regions, including the roofs, underground backfill pillars, and the slopes can be guaranteed during OPB.

The proposed method is utilized in waste tailings disposal and the OPB in a safe way, which can provide valuable suggestions for open-pit metal mines with similar situations. Simultaneously, the findings of this study provided a practical basis for the OPB in the future, which can treat solid waste resources to a large extent and realize safe production. Tailings, ordinary Portland cement 425#, and tap water, as aggregates, cementitious materials and mixing agent, respectively, are recommended for practical use of CPB. In the actual mixed design of CPB, it is necessary for engineers to detect the chemical composition of tailings to prevent danger to the environment and humans.

However, the results of the present study are restricted to the selection of the proportion of similar materials for the OPB and proportions of CPB components in practical application have not been determined so as to obtain optimized strengths, which can be further studied in future research.

Supplementary Materials: The following are available online at <https://www.mdpi.com/article/10.3390/min11080818/s1>, Table S1: Backfill parameters of the open pit implemented previously; Table S2: Uniform design ratios; Table S3: Results of uniform parameter tests; Table S4: Simulation results of safety factors of roofs and underground backfill pillars.

Author Contributions: Writing—original draft preparation, Q.Z. and B.Z.; data curation, B.Z. and D.W.; conceptualization, Q.Z. and B.Z.; methodology, Q.C., D.W. and X.G.; software, Q.Z., X.G. and Q.C.; validation, B.Z. and Q.C.; writing—review and editing, Q.Z. and B.Z.; supervision, Q.C.; funding acquisition, Q.Z. All authors have read and agreed to the published version of the manuscript.

Funding: This research was funded by Hunan Provincial Natural Science Foundation Project (No. 2020JJ5718), and the National Science Foundations of China (No. 52074351 and No. 52004330).

Acknowledgments: The authors would like to thank Hengliang Liu, Shihua Dong, and Weihong Su for funding support in the project, and Yikai Liu for technical support in the writing process.

Conflicts of Interest: The authors declare no conflict of interest.

References

1. King, B.; Goycoolea, M.; Newman, A. Optimizing the open pit-to-underground mining transition. *Eur. J. Oper. Res.* **2017**, *257*, 297–309. [[CrossRef](#)]
2. Dos Santos, T.B.; Lana, M.S.; Pereira, T.M.; Canbulat, I. Quantitative hazard assessment system (Has-Q) for open pit mine slopes. *Int. J. Min. Sci. Technol.* **2019**, *29*, 419–427. [[CrossRef](#)]
3. Qi, C.; Fourie, A. Cemented paste backfill for mineral tailings management: Review and future perspectives. *Miner. Eng.* **2019**, *144*, 106025. [[CrossRef](#)]
4. Wang, Q.; Li, J.; Zhu, X.; Yao, G.; Wu, P.; Wang, Z.; Lyu, X.; Hu, S.; Qiu, J.; Chen, P.; et al. Approach to the management of gold ore tailings via its application in cement production. *J. Clean. Prod.* **2020**, *269*, 122303. [[CrossRef](#)]
5. Sun, W.; Wang, H.; Hou, K. Control of waste rock-tailings paste backfill for active mining subsidence areas. *J. Clean. Prod.* **2018**, *171*, 567–579. [[CrossRef](#)]
6. Rimélé, M.A.; Dimitrakopoulos, R.; Gamache, M. A stochastic optimization method with in-pit waste and tailings disposal for open pit life-of-mine production planning. *Resour. Policy* **2018**, *57*, 112–121. [[CrossRef](#)]

7. Dong, K.; Xie, F.; Wang, W.; Chang, Y.; Lu, D.; Gu, X.; Chen, C. The detoxification and utilization of cyanide tailings: A critical review. *J. Clean. Prod.* **2021**, *302*, 126946. [[CrossRef](#)]
8. Chakilam, S.; Cui, L. Effect of polypropylene fiber content and fiber length on the saturated hydraulic conductivity of hydrating cemented paste backfill. *Constr. Build. Mater.* **2020**, *262*, 120854. [[CrossRef](#)]
9. Qi, C.; Fourie, A.; Chen, Q.; Zhang, Q. A strength prediction model using artificial intelligence for recycling waste tailings as cemented paste backfill. *J. Clean. Prod.* **2018**, *183*, 566–578. [[CrossRef](#)]
10. Benzaazoua, M.; Bussière, B.; Demers, L.; Aubertin, M.; Fried, É.; Blier, A. Integrated mine tailings management by combining environmental desulphurization and cemented paste backfill: Application to mine Doyon, Quebec, Canada. *Min. Eng.* **2008**, *21*, 330–340. [[CrossRef](#)]
11. Bastola, S.; Cai, M.; Damjanac, B. Slope stability assessment of an open pit using lattice-spring-based synthetic rock mass (LS-SRM) modeling approach. *J. Rock Mech. Geotech. Eng.* **2020**, *12*. [[CrossRef](#)]
12. Paul, S. Finite Element Analysis in Fused Deposition Modeling Research: A Literature Review. *Measurement* **2021**, *178*, 109320. [[CrossRef](#)]
13. Tu, H.; Zhou, H.; Lu, J.; Gao, Y.; Shi, L. Elastoplastic coupling analysis of high-strength concrete based on tests and the Mohr-Coulomb criterion. *Constr. Build. Mater.* **2020**, *255*, 119375. [[CrossRef](#)]
14. Zhang, J.; Wang, Z.; Song, Z. Numerical study on movement of dynamic strata in combined open-pit and under-ground mining based on similar material simulation experiment. *Arab. J. Geosci.* **2020**, *13*, 785. [[CrossRef](#)]
15. Wang, J.; Ren, L.; Xie, L.; Xie, H.; Ai, T. Maximum mean principal stress criterion for three-dimensional brittle fracture. *Int. J. Solids Struct.* **2016**, *102*, 142–154. [[CrossRef](#)]
16. Liu, B.; Zhou, J.; Wen, X.; Guo, J.; Deng, Z.; Hu, X. Mechanical performance and failure criterion of coral concrete under combined compression-shear stresses. *Constr. Build. Mater.* **2021**, *288*, 123050. [[CrossRef](#)]
17. Ma, D.; Zhang, J.; Duan, H.; Huang, Y.; Li, M.; Sun, Q.; Zhou, N. Reutilization of gangue wastes in underground backfilling mining: Overburden aquifer protection. *Chemosphere* **2021**, *264*, 128400. [[CrossRef](#)]
18. Khaboushan, A.S.; Osanloo, M.; Esfahanipour, A. Optimization of open pit to underground transition depth: An idea for reducing waste rock contamination while maximizing economic benefits. *J. Clean. Prod.* **2020**, *277*, 123530. [[CrossRef](#)]
19. Tian, Q.; Zhang, J.; Zhang, Y. Similar simulation experiment of expressway tunnel in karst area. *Constr. Build. Mater.* **2018**, *176*, 1–13. [[CrossRef](#)]
20. Tao, Z.; Shu, Y.; Yang, X.; Peng, Y.; Chen, Q.; Zhang, H. Physical model test study on shear strength characteristics of slope sliding surface in Nanfen open-pit mine. *Int. J. Min. Sci. Technol.* **2020**, *30*, 421–429. [[CrossRef](#)]
21. Li, Y.; She, L.; Wen, L.; Zhang, Q. Sensitivity analysis of drilling parameters in rock rotary drilling process based on orthogonal test method. *Eng. Geol.* **2020**, *270*, 105576. [[CrossRef](#)]
22. Morris, S.; Jackson, I. Implications of the similarity principle relating creep and attenuation in finely grained solids. *Mater. Sci. Eng. A* **2009**, *521*, 124–127. [[CrossRef](#)]
23. Han, C.; Zhang, J. Study on well hard shut-in experiment based on similarity principle and erosion of ram rubber. *Eng. Fail. Anal.* **2013**, *32*, 202–208. [[CrossRef](#)]
24. Ning, J.-H.; Zhou, Y.-D.; Fang, K.-T. Discrepancy for uniform design of experiments with mixtures. *J. Stat. Plan. Inference* **2011**, *141*, 1487–1496. [[CrossRef](#)]
25. Feng, Y.; Yang, Q.; Chen, Q.; Kero, J.; Andersson, A.; Ahmed, H.; Engström, F.; Samuelsson, C. Characterization and evaluation of the pozzolanic activity of granulated copper slag modified with CaO. *J. Clean. Prod.* **2019**, *232*, 1112–1120. [[CrossRef](#)]
26. Cardoso, V.H.; Caldas, P.; Giraldo, M.T.R.; Frazão, O.; de Carvalho, C.J.R.; Costa, J.C.; Santos, J.L. Experimental investigation of a strain gauge sensor based on Fiber Bragg Grating for diameter measurement. *Opt. Fiber Technol.* **2021**, *61*, 102428. [[CrossRef](#)]
27. Naik, A.B.; Reddy, A.C. Optimization of tensile strength in TIG welding using the Taguchi method and analysis of variance (ANOVA). *Therm. Sci. Eng. Prog.* **2018**, *8*, 327–339. [[CrossRef](#)]
28. Sei, T.; Shibata, H.; Takemura, A.; Ohara, K.; Takayama, N. Properties and applications of Fisher distribution on the rotation group. *J. Multivar. Anal.* **2013**, *116*, 440–455. [[CrossRef](#)]
29. Huang, G.; Kulatilake, P.H.; Shreedharan, S.; Cai, S.; Song, H. 3-D discontinuum numerical modeling of subsidence incorporating ore extraction and backfilling operations in an underground iron mine in China. *Int. J. Min. Sci. Technol.* **2017**, *27*, 191–201. [[CrossRef](#)]
30. Zingano, A.; Weiss, A. Subsidence over room and pillar retreat mining in a low coal seam. *Int. J. Min. Sci. Technol.* **2019**, *29*, 51–57. [[CrossRef](#)]
31. Hai, P.; Jian, Z. Research on protecting the safety of buildings by using backfill mining with solid. *Procedia Environ. Sci.* **2012**, *12*, 191–198. [[CrossRef](#)]
32. Lu, Y.; Li, M.; Wang, D.; Shi, X.; Li, H.; Zhu, Y.; Ye, Q.; Lu, J. Discharge and ignition characteristics from indentation fracture of coal mine roof. *Fuel* **2021**, *291*, 120208. [[CrossRef](#)]
33. Asem, P.; Gardoni, P. Bayesian estimation of the normal and shear stiffness for rock sockets in weak sedimentary rocks. *Int. J. Rock Mech. Min. Sci.* **2019**, *124*, 104129. [[CrossRef](#)]
34. Su, Z.; Shao, L. A three-dimensional slope stability analysis method based on finite element method stress analysis. *Eng. Geol.* **2021**, *280*, 105910. [[CrossRef](#)]

35. Kinakin, D.; Stead, D. Analysis of the distributions of stress in natural ridge forms: Implications for the deformation mechanisms of rock slopes and the formation of sackung. *Geomorphology* **2005**, *65*, 85–100. [[CrossRef](#)]
36. Wu, Z.; Chen, C.; Lu, X.; Pei, L.; Zhang, L. Discussion on the allowable safety factor of slope stability for high rockfill dams in China. *Eng. Geol.* **2020**, *272*, 105666. [[CrossRef](#)]
37. Zheng, J.; Li, L. Experimental study of the “short-term” pressures of uncemented paste backfill with different solid contents for barricade design. *J. Clean. Prod.* **2020**, *275*, 123068. [[CrossRef](#)]
38. Zhang, Q.; Li, Y.; Chen, Q.; Liu, Y.; Feng, Y.; Wang, D. Effects of temperatures and pH values on rheological properties of cemented paste backfill. *J. Cent. South Univ.* **2021**, *28*, 1707–1723. Available online: <https://kns.cnki.net/kcms/detail/43.1516.tb.20210318.1429.002.html> (accessed on 27 July 2021). [[CrossRef](#)]
39. Xu, W.-B.; Liu, B.; Wu, W.-L. Strength and deformation behaviors of cemented tailings backfill under triaxial compression. *J. Central South Univ.* **2020**, *27*, 3531–3543. [[CrossRef](#)]
40. Guo, Y.-X.; Ran, H.-Y.; Feng, G.-R.; Du, X.-J.; Qi, T.-Y.; Wang, Z.-H. Effects of curing under step-by-step load on mechanical and deformation properties of cemented gangue backfill column. *J. Central South Univ.* **2020**, *27*, 3417–3435. [[CrossRef](#)]
41. Chen, Q.; Sun, S.; Liu, Y.; Qi, C.; Zhou, H.; Zhang, Q. Experimental and numerical study on immobilization and leaching characteristics of fluoride from phos-phogypsum based cemented paste backfill. *Int. J. Min. Metall. Mater.* **2021**. [[CrossRef](#)]
42. Li, X.; Peng, K.; Peng, J.; Xu, H. Effect of Cyclic Wetting–Drying Treatment on Strength and Failure Behavior of Two Quartz-Rich Sandstones under Direct Shear. *Rock Mech. Rock Eng.* **2021**. [[CrossRef](#)]